Lab on a Chip

PAPER

View Article Online
View Journal | View Issue

Cite this: *Lab Chip*, 2025, **25**, 69

Flow cell for high throughput Raman spectroscopy of non-transparent solutions†

Filippo Zorzi, [ab] Emil Alstrup Jensen, [cd] Murat Serhatlioglu, [d] Silvio Bonfadini, [a] Morten Hanefeld Dziegiel, [ce] Luigino Criante *[a] and Anders Kristensen [d]

Received 10th July 2024,
Accepted 26th November 2024

DOI: 10.1039/d4lc00586d

rsc.li/loc

This work introduces a high-throughput setup for Raman analysis of various flowing fluids, both transparent and non-transparent. The setup employs a microfluidic cell, used with an external optical setup, to control the sample flow's position and dimensions *via* 3-dimensional hydrodynamic focusing. This approach, in contrast to the prevalent use of fused silica capillaries, reduces the risk of sample photodegradation and boosts measurement efficiency, enhancing overall system throughput. The microfluidic cell has been further evolved to laminate two distinct flows from different samples in parallel. Using line excitation, both samples can be simultaneously excited without moving parts, further increasing throughput. This setup also enables real-time monitoring of phenomena like mixing or potential reactions between the two fluids. This development could significantly advance the creation of highly sensitive, high-throughput sensors for fluid composition analysis.

Introduction

Raman spectroscopy (RS) is a non-invasive, non-destructive technique that identifies chemical compounds by analyzing their molecular energy spectrum *via* inelastic scattering of light. Its highly sensitive and non-labeling characteristics make it particularly attractive for biomedical and biosensing applications, as it allows for the examination of processes at the single-cell level without disturbing the cellular environment.

With its unique analysis characteristics, RS has found extensive use across various fields. Since the seminal 1972 study on hemoglobin and erythrocytes,[1] it has been utilized in bioanalytics and blood analysis. It has also proven effective in identifying numerous disease-related biomarkers.[2–4] However, its clinical applications has been significantly limited by two major drawbacks. Firstly, many studies involving RS on biological samples necessitate time-consuming sample preparation of about 40–60 minutes. Secondly, the inherent weakness of the Stokes component in spontaneous RS requires an extended integration time to gather an adequate signal. Considering the Raman scattering efficiency, it is estimated that only one in every 10^8 photons undergoes inelastic scattering during its interaction with matter.[5–7] For single-cell analysis, common methods include smearing the sample on a glass substrate[8–10] and optical trapping.[11,12] However, these methods necessitate lengthy preparation times due to steps like pre-treatment and sample centrifugation, slowing the overall process. Additionally, signal collection from a large number of cells is time-consuming.

In addition, when using static samples, prolonged exposure times can cause photodegradation or thermal damage, irreversibly affecting the measurement. To mitigate this, one typical solution is to use a source in the NIR region (usually 785 nm) for optical excitation in Raman analysis. This range offers low light absorption for biological samples, significantly reducing potential radiation damage. However, as the Raman signal intensity is proportional to $1/\lambda^4$,[13,14] using these wavelengths results in a lower signal compared to visible wavelengths. Consequently, longer integration times are required to achieve a good signal-to-noise ratio, leading to low device throughput. Performing Raman spectroscopy on flowing samples is another potential solution to avoid photodegradation.

Other optical detection methods for flowing cells in a fluidic unit rely on the fluorescence emitted by fluorophores within the cells and/or scattering of light at different angles as the excitation light interacts with the cells being analyzed.[15,16] Although these methods generally provide significantly greater intensity than the

[a] *Center for Nano Science and Technology, Istituto Italiano di Tecnologia, Via Rubattino, 20134, Milan, Italy. E-mail: luigino.criante@iit.it*
[b] *Department of Physics, Politecnico di Milano, Piazza Leonardo da Vinci, 32, 20133, Milano, Italy*
[c] *Department of Clinical Immunology, Copenhagen University Hospital, Blegdamsvej 9, Section A DK-2100 Copenhagen Ø, Denmark*
[d] *Department of Health Technology, Danmarks Tekniske Universitet, Ørsteds Plads, Building 345C DK-2800 Kgs. Lyngby, Denmark*
[e] *Department of Clinical Medicine, Københavns Universitet, Blegdamsvej 3B 33.5, Section A DK-2200 Copenhagen, Denmark*

† Electronic supplementary information (ESI) available. See DOI: **https://doi.org/10.1039/d4lc00586d**

Raman emission (typically due to fluorophores with very strong emission or scattering from metallic labels), they offer limited information about the samples' molecular fingerprint. Fluorescence intensity is proportional to the amount of fluorophore entering or being attached to the cell. Light scattering at different angles is mainly related to geometrical parameters such as cell size, morphology, and roughness;[17] Metallic labels and fluorophores are costly and could destroy cell integrity, and the sample is often not reusable. In addition, only Raman spectroscopy can provide complete information about the sample's chemical composition based on molecular vibrational modes, giving a molecular fingerprint. These factors make Raman spectroscopy unparalleled in the quantity and quality of information it can provide about a given sample in a non-invasive and label-free manner. When examining whole blood, the prevalent method typically involves using fused silica capillaries as "sample holder".[18–23] Given the high viscosity of blood, a capillary diameter of at least 100 μm is necessary to prevent clogging. However, due to the pump laser beam's typical focal spot size (up to tens of microns), only a minuscule percentage of the total sample can be analyzed. Furthermore, the pump beam's penetration depth is restricted by the scattering caused by blood's corpuscular nature. Consequently, even if the sample is scanned with moving parts to increase the analysis area, the measurement is confined to the sample portion near the capillary's glass walls. This situation presents a dual disadvantage: firstly, the useful Raman signal may not be representative as it originates from the sample part experiencing the highest shear stress due to the gradient of the fluid's parabolic velocity profile; secondly, the substrate's background signal is amplified. This unfortunate combination of factors negatively impacts the signal-to-noise ratio, occasionally rendering the measurement unfeasible.

In recent years, various flow cytometers have been proposed in the literature capable of acquiring Raman spectra of flowing single cells.[24–27] However these devices, due to the brief interaction between cells and light, employ coherent Raman scattering techniques (such as CARS or SERS) that necessitate intricate optical setups.

These challenges significantly restrict the applicability of Raman spectroscopy in the clinic, where the ability to rapidly analyze a sample is often crucial.

In this paper, we introduce an innovative lab-on-a-chip platform that improves flow sample analysis throughput, especially for corpuscular and non-transparent sample such as blood, by enabling simultaneous multi-stream Raman spectroscopy. Leveraging the fluid control capabilities of a 3D microfluidic geometry, we can conduct quick and efficient Raman measurements of flowing blood with virtually no sample preparation time, using a visible excitation wavelength.

Materials and methods

Design of microfluidic chip

The lab-on-a-chip (LoC) design employs three-dimensional hydrodynamic focusing. An innovative two-inlet geometry[28] laminates and centers the sample stream in the outer microfluidic channel for Raman signal collection (Fig. 1). The sample, entirely encased by a buffer sheath, is analyzed. A significant decrease in Raman signal intensity was observed with an increase in the glass layer thickness between the objective lens and the measurement region. To enhance signal collection efficiency, a recess was created to reduce the glass thickness to 50 μm in the analysis area. The buffer inlet, analyte inlet, and output channel all have a square cross-section, with sides of 300 μm, 80 μm, and 150 μm, respectively. The chip dimensions are 3.5 × 2 mm. The simplicity of the geometry allows for easy adjustment of the sample flow size by controlling the pressure ratio between the two inlets, resulting in a minimum size of 15 μm (Fig. 2). This unique feature allows the stream size to match the Raman excitation voxel size. Therefore, the analysis of 100% of the blood passing through the channel can be analysed, as the Raman signal from the entire sample volume is collected (Fig. 4). Additionally, the sample fluid's location away from the channel walls significantly reduces the background signal from the fused silica walls.

By reducing the sample flow diameter by roughly a factor of ten, the flow velocity significantly increases compared to the capillary. The velocity at the interface between the two fluids (sample and buffer) is typically uniform, minimizing shear stress, and its profile at the center is nearly constant. This results in cells being less affected by the wall lift force, which otherwise pushes them away from the wall, creating a cell concentration gradient that hampers measurement efficiency. The increased flow speed enables signal collection from a larger number of cells within the same measurement integration time, enhancing the device's throughput compared to state-of-the-art methods. Additionally, the interaction time between the single cell and the laser beam is reduced, allowing for a more powerful Raman pump signal without triggering photodegradation. The lower energy transferred to the cell and the effective heat extraction from the measurement area by intrinsic fluid dynamic mechanisms shift the damage threshold to higher values. Raman excitation of whole blood with green light becomes possible, improving the intensity of the collected signal since Raman signal intensity is proportional to $1/\lambda^4$. This enables a good signal-to-noise ratio even with short integration times, down to less than 1 s. Furthermore, our platform, thanks to the innovative chip manufacturing process, allows for sample stream multiplexing, enabling simultaneous analysis of more than one blood sample. When coupled with an optical system involving line excitation and an imaging spectrometer, it allows for the simultaneous collection of several Raman spectra without the need for moving parts inside the setup. An analysis throughput of more than one hundred whole blood samples per hour can potentially be achieved.

Fabrication process

The microfluidic chip was fabricated using the FLICE (*femtosecond laser irradiation followed by chemical etching*) method, a renowned technique for rapidly creating 3D

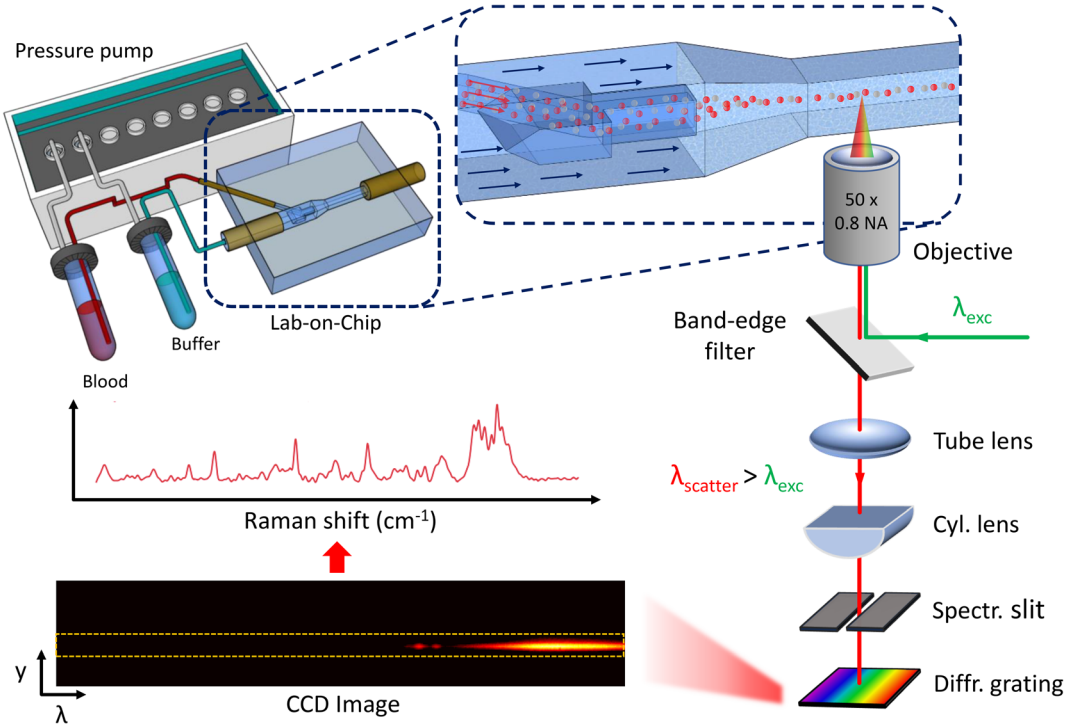

Fig. 1 Schematic of the experimental setup. A pressure pump controls the focusing of the particles inside the Lab-on-a-Chip. The excitation light is focalized inside the chip *via* an objective, also used to collect the scattered light. This scattered light is reflected by a dichroic mirror and, after passing through a notch filter, is sent to the CCD camera inside a spectrometer, that enables us to extract the Raman spectra.

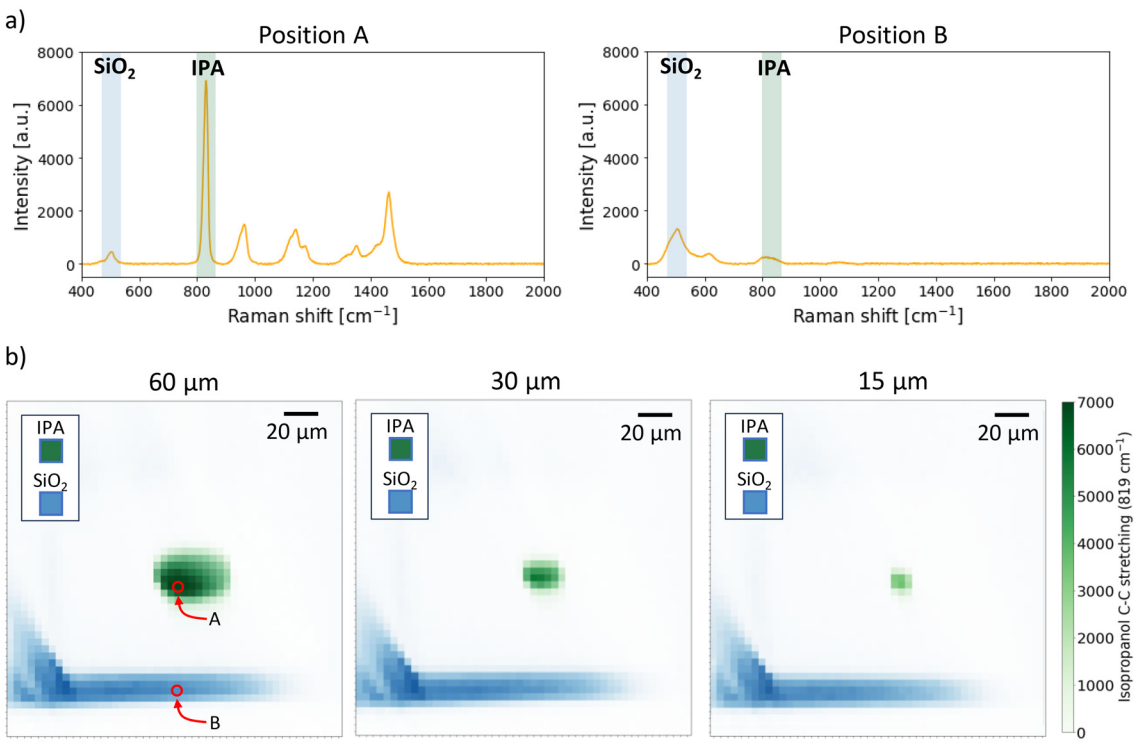

Fig. 2 a) Raman spectra obtained using isopropanol (IPA) in the sample inlet and MilliQ water in the buffer inlet, taken in positions A and B shown in Fig. 2b, with 532 nm as excitation wavelength and integration time of 1 s. The intensity of two peaks was tracked for each position: the IPA peak at 819 cm^{-1} and the SiO_2 peak at 465 cm^{-1}. b) Raman intensity maps of channel cross-section with focused isopropanol. It is possible to change the size of the focused stream by changing the pressure ratio between the sample inlet and the buffer inlet and match it with the voxel size of the objective lens.

geometries fully buried within a transparent glass substrate.[29–33] This method involves two steps. In the first step, a geometry is inscribed inside the fused silica substrate using femtosecond laser irradiation. Non-linear interactions between the photons and the substrate lattice allow for substrate modification solely at the beam's focal spot, thereby avoiding harmful thermal effects. The specific energy range of the laser pulse used, combined with the write beam polarisation, induces and aligns nanocracks within the substrate, that enhance the etching rate of the inscribed parts.

The second harmonic of an ultrashort pulsed laser (PHAROS PH2-10W, LightConversion) was used. Fabrication was achieved by focusing the laser beam with 420 nJ pulses through an objective (50× M Plano APO NIR, Mitutoyo) inside the fused silica substrate (Fused silica, FOCKtech). The substrate was placed on a high-precision, 3-axis air bearings stage (Fiber-Clide3D, Aerotech), controlled by a CAD-based software (SCA, Altechna). The stage speed was set to 1 mm s^{-1} when the laser beam was on, and 10 mm s^{-1} when the laser beam was off. The beam polarization was perpendicular to the writing direction to maximize the etching rate.[34] Precise 3D geometries were written inside the substrate by moving the stage.

In the second step, the substrate is subjected to wet chemical etching to selectively remove the laser-modified parts in an aqueous 20% hydrofluoric acid solution at a controlled temperature of 35 °C. The etching rate in the laser-written parts of the glass increases to around 700 μm h^{-1}, while the unwritten parts will etch at a lower rate of about 20 μm h^{-1}. This selective glass removal enables the creation of 3D monolithic microfluidic circuits fully embedded within the fused silica substrate.[35–37] The rigidity and inertness of fused silica allow for indefinite platform reuse following proper cleaning.

In order to optimize the performances of the microfluidic system, some useful expedients have been adopted in the design and assembly process (refer to ESI† S1).

Microfluidics

Flow rates in the microfluidic chip were controlled using a pressure pump (FLUIGENT MFCS Flex), connected to vials serving as sample and buffer reservoirs, which were connected to the chip. The flow rate was monitored using flow sensors (FLUIGENT FLOW UNIT M for the sample, FLUIGENT FLOW UNIT XL for the buffer), connected in series downstream of the fluid reservoirs.

Raman spectroscopy setup

The optical setup employs a 532 nm continuous wave laser source (Cobolt 08-01 Series), focused inside the microchannels with a 50×, 0.8 NA objective. This objective focuses the beam into a spot of 2.86 μm and a depth of focus of 20 μm, measured using the razor-edge method. The same objective collects the Stokes Raman scattered light, separated from the pump light with a dichroic mirror. After passing through a long-pass edge filter and a notch filter to eliminate residual signals from Rayleigh scattering, the light is analyzed with an imaging spectrometer (ANDOR Shamrock SR-500i) set with a 300 μm wide slit. The wavelengths are separated with a 1200 lines per mm diffraction grating, and the light is directed into a highly-sensitive CCD camera (Newton 920), cooled to −70 °C to reduce thermal background. The Raman spectrum of the analyzed sample is extracted from the CCD image (Fig. 1).

Sample preparation

Preliminary measurements were conducted using isopropanol in the sample channel, and MilliQ water in the buffer channel, both of which were filtered prior to use. Whole blood samples, provided by Copenhagen University Hospital in EDTA tubes, were stored at 4 °C, with no sample preparation before use. Here, the buffer solution was consisted of 1000 × 0.5 mM EDTA mixed with phosphate buffered saline (PBS) in a 1 : 1000 ratio.

Ethical approval

Blood was collected from voluntary blood donors after obtaining informed written consent for use of blood as normal material. Samples were anonymized and accompanied by reference data. According to legislation, this use of anonymized donor samples as normal material does not require approval by an ethical committee.

Results and discussion

Single inlet chip

A significant advantage to our platform is the ability to adjust the flow focusing size of the sample by controlling the sheath/sample pressure ratio (Fig. 2). The flow focusing size can be reduced to 15 μm and consistently matched with the size of the Raman laser excitation voxel, without the risk of clogging. This allows for signal collection from the entire sample volume with a single measurement. The Raman maps in Fig. 2 were obtained using isopropanol (IPA) in the sample inlet, and water in the buffer inlet. The integration time was set to 1 s. A single Raman spectrum was collected for each new position of the laser excitation voxel (step size: 5 μm) and the intensity of the isopropanol peak with Raman shift of 819 cm^{-1} was tracked. The fused silica peak at 465 cm^{-1} was tracked in the inlets.

Given that the Raman signal intensity is proportional to the analyte concentration,[38,39] our platform can associate intensity with a specific number of molecules interrogated by the excitation beam for a set integration time. To test this, isopropanol at varying concentrations was used as a test analyte (Fig. 3). By maintaining a constant flow focusing rate, the flow size and position of the excitation beam, which was optimized to maximize signal collection, remained constant across all measurements. For each integration time, a spectrum was taken with the focused flow of IPA surrounded by water, followed by a spectrum with only water in the channel. After subtracting the two spectra, the intensity of

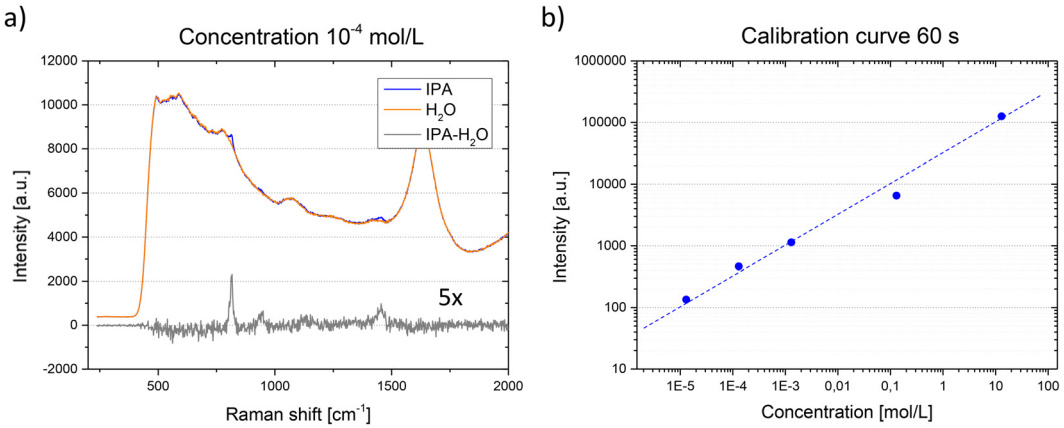

Fig. 3 a) Raman spectra obtained collecting the signal from a focalized stream of a water dilution of IPA at a concentration of 10^{-4} mol l^{-1}, surrounded by water (light blue) and by having only water in the channel (orange). As can be seen from the difference between the two spectra (grey, magnified by a factor 5), the presence of IPA is detectable. b) Calibration curve that correlates the concentration of IPA to the intensity of the peak detected at 819 cm^{-1}.

the IPA peak corresponding to a Raman shift of 819 cm^{-1} was plotted. This enabled the creation of a calibration curve (Fig. 3b), associating a given isopropanol concentration with a specific signal intensity. Consequently, a useful signal down to a concentration of 13 μmol l^{-1} was obtained using an exposure time of 60 s.

This method is applicable to any fluid type including nontransparent or corpuscular fluids, without compromising measurement effectiveness. A comparison between the capillary and the microfluidic chip can be observed when using blood group A whole blood as analyte (Fig. 4a). In this case, the intensities of the fused silica peak at 465 cm^{-1} and a hemoglobin peak, at 1580 cm^{-1}, were plotted (Fig. 4b). Due to blood's corpuscular nature, the penetration depth of the beam inside the capillary is limited to 15 μm, restricting measurement efficiency as only about 8% of the total volume flowing into the capillary can be interrogated. Additionally, measurements performed close to the wall always present significant background signal from the fused silica. Conversely, with the microfluidic chip, we can collect the signal from 100% of the blood volume flowing through the channel, virtually eliminating the fused silica's background noise (Fig. 4c). This geometry allows each cell flowing in the channel to be interrogated by the pump beam, enhancing measurement effectiveness. This is particularly crucial considering that some diseases are associated with the presence of rare cells within the blood.[40,41]

Measurements are made where the fluid flow is focused, specifically in the center of the microchannel. Given the laminar regime of the fluid flow in the channel, its velocity profile exhibits a parabolic pattern, with the minimum velocity near the wall and the maximum at the channel center. This results in a minimal (approximately zero) velocity gradient where the sample fluid is focused, leading to fairly uniform cell velocity. This is crucial as it ensures all cells are scanned by the beam for similar time intervals, yielding signals of comparable intensity. As shear stress on the cells is directly proportional to the velocity gradient, it is also minimal. Unlike in a capillary, the lift force on the cells is zero and no cell concentration gradient forms in the analysis zone, enhancing the robustness of the measurement. A further advantage of this geometry is minimal sample consumption during the measurements. The flow rate inside the sample and buffer channels was measured for different focusing sizes using filtered isopropanol. With a cross-section of approximately 20 × 20 μm, the flow rate inside the sample channel reached 2 μl min^{-1}, while the buffer inlet was 310 μl min^{-1}. The spectra collection for these maps took about 45 minutes in total, implying that these complete scans were conducted using a total sample volume of 100 μl.

The cell flow speed in the channel is significantly higher compared to a capillary. For a flow rate of 2 μl min^{-1} and a cross-section of 20 × 20 μm, the average speed is 8.2 cm s^{-1}, marking an increase by a factor of 19.3 compared to a capillary with a diameter of 100 μm. As previously mentioned, the velocity profile is nearly uniform. The volume of blood analyzed in a given time interval increases by the same factor. Specifically, under the same conditions, the volume changes from 0.015 μl analyzed per minute with the capillary to μl analyzed with the lab-on-chip. The number of cells analyzed per minute increases from 75 × 10^3 with the capillary to 1.5 × 10^6 with the hydrodynamic focusing chip (additional details in the ESI† S2). Despite a shorter interaction time between cells and the excitation beam yielding a weaker signal from individual cells, the increased number of cells analyzed per unit of time allows for signal collection averaged over a larger, and thus more statistically significant, sample. Reducing the interaction time between cells and the beam allows for an increase in laser power without causing cell photodegradation. To quantify this increase, power measurements were conducted with two different device configurations using the same blood sample. Excitation was consistently performed with a 532 nm CW laser. However, by employing neutral density filters with

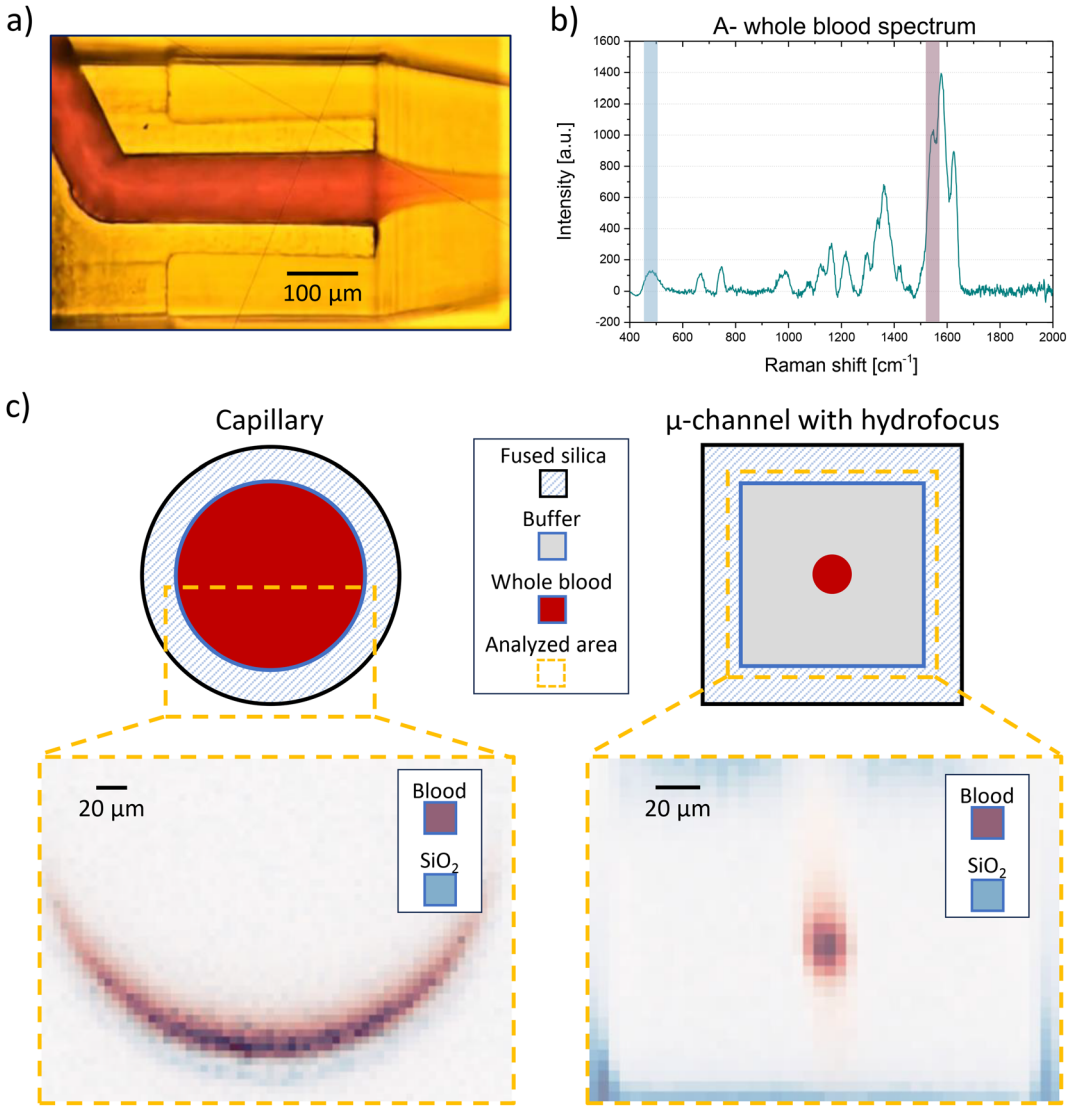

Fig. 4 a) Microscope image of the single hydrodynamic focusing chip used with whole blood in the sample inlet and PBS in the buffer inlet. b) Blood group A– blood spectrum. The two tracked peaks of the 2D maps in figure a have been highlighted. c) Analyzed regions in the capillary and in the hydrodynamic focusing, using whole blood. Using the capillary the signal is collected from only 8% of the total volume, while with the chip the signal can be collected from the entire volume of the sample.

varying absorption (THORLABS, NDK01), the laser intensity was adjusted from 0.8 kW cm^{-2} to 1675 kW cm^{-2}. The Raman signal was collected using a 50× objective with an integration time of 1 s. The amplitude of two different peaks was then tracked and plotted as a function of laser intensity.

The use of the lab-on-a-chip allows for a six-fold increase in excitation intensity without cell photodegradation (up to 265 kW cm^{-2}), and an overall signal increase by a factor of 1.5 (see ESI† S3). Unlike the capillary, exceeding the density power photodegradation threshold does not alter the spectrum, and degraded or burned cells do not tend to adhere to the channel's edge, an event that would necessitate thorough device cleaning and compromise the measurement. Instead, these cells are transported away from the analysis zone, simplifying device usage. This configuration offers a dual advantage: it not only enables measurements on a larger number of cells within the same measurement time but also allows for higher power measurements without risking sample damage due to lower photodegradation, ultimately enabling faster measurements with integration times shorter than 1 s.

While no significant structural damage to the red blood cells is observable in the channel, spectra reveal an increased degree of deoxygenation as power increases. Even at low powers, visible Raman excitation can initially trigger oxygen photo-dissociation from hemoglobin.[42] The Raman peak intensity at 1547 cm^{-1} rises while the intensity at 1585 cm^{-1} falls, indicating a transition of Fe from a low-spin to a high-spin state. Owing to the shorter interaction time between cells and the beam in the channel compared to the capillary, the deoxygenation rate is much slower with increasing laser power, facilitating easier measurement control (see ESI† S3).

The flow rate can be adjusted by the sheath and sample inlet pressure ratio, while keeping the size of the sample stream constant. This means that flow rate and laser power can be chosen in unison such that the state of the sample can be easily controlled (*e.g.* deoxygenation state), while maintaining a high throughput and favourable signal-to-noise ratio (see ESI† S4).

Two inlets chip

It is crucial to enhance the device's throughput further, as comprehensive blood tests analyzing multiple parameters simultaneously are vital in blood banking[23] and for diagnosing or predicting various diseases. Standard methods for comprehensive analysis are time-consuming and require extensive sample preparation. The use of the LoC offers significant advantages over the analysis of static samples or capillary analysis of moving samples, including scalability, which is useful for increasing device throughput. In addition, its unique 3D geometry solution for a user-friendly hydrodynamic focusing allows the signal to be collected from the entire volume of blood passing through the channel, improving measurement efficiency and enabling faster analysis due to the increased photodegradation threshold. Most chip-making geometries for hydrodynamic focusing are complex and do not allow for side-by-side multiple flows. The configuration used here can be easily modified to laminate two fluid flows in parallel, effectively doubling the device's throughput (Fig. 5a). To increase the measurement's throughput, it is necessary to simultaneously

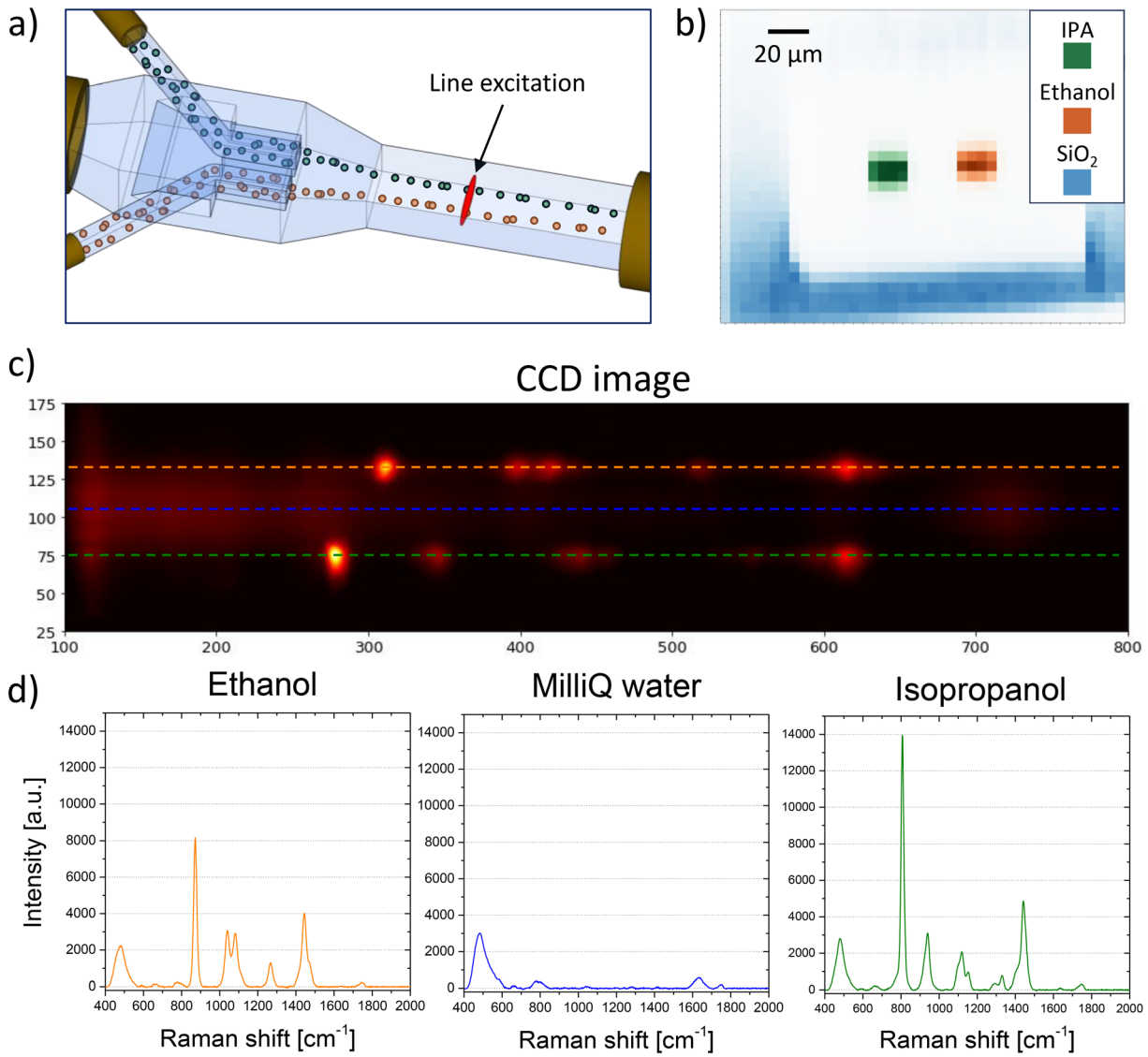

Fig. 5 a) Schematic drawing of the double inlet chip. b) 2D scan obtained with the double inlet chip using IPA (green) and ethanol (orange) in the two sample inlets. It has been tracked the peak at 819 cm^{-1} for IPA, the peak at 883 cm^{-1} for ethanol, and at 465 cm^{-1} for fused silica. c) CCD image obtained using line excitation (30 s integration time) and the double inlet chip, with IPA (green) and ethanol (orange) in the two sample inlets. d) The respective spectra can be obtained by plotting the CCD intensity on different horizontal lines.

collect the signal from the different fluids. A simple method was developed to collect these spectra without the need for moving parts in the setup. The excitation laser beam was shaped with a cylindrical lens placed before the 50× objective lens to transform the excitation spot into a line. This allows for the simultaneous excitation and collection of the Raman signal from both fluids. When isopropanol and ethanol are used in the two sample inlets, the signal from the two analytes can be easily distinguished (Fig. 5b). From the CCD-obtained image, the spectra of ethanol and IPA can be extracted by analyzing the image intensity along two horizontal lines in two different image areas (Fig. 5c and d). The presence of mixing between the two fluids can be immediately detected by checking for their characteristic peaks in the region between the two. As observed, due to the flow's laminarity no mixing occurs between the two fluids (blue horizontal line in Fig. 5c and the corresponding spectrum in Fig. 5d), which remain well separated.

Line excitation offers another advantage, observable when analyzing the signal as a function of the *y*-coordinate of the CCD. As the *y*-axis of the CCD image represents the spatial extent of the excitation line, tracking the evolution of peaks of interest along the *y*-axis enables extraction of increased spatial resolution information about the analyzed fluid, compared to point excitation. Given that the field of view of the objective lens is 100 μm and occupies about 200 pixels on the CCD, this method achieves a spatial resolution in the excitation line direction of about 500 nm, close to the diffraction limit of the objective, proportional to $\lambda/2n$, with n being the refractive index of the material. Considering that the spot size of the 50× objective is 3 μm and sets the resolution limit, this method can enhance the spatial resolution six-fold compared to a point-by-point scan. Furthermore, this method allows for a scan with a single measurement without the need for moving parts, unlike a point-like spot which would require stage movement for the same scan. This method has several applications. By knowing the fluid velocity inside the channel and analyzing the profile evolution of different peaks along the channel length, it is possible to determine the diffusion constant of the fluid or its different components inside the buffer. This is particularly important for fluids like blood, which contains different components that can diffuse differently. When using different fluids, real-time monitoring of their reactions with each other and evaluation of the reaction speed are possible. Lastly, real-time observation of how two different fluids mix together is achievable.

After successfully testing the device with isopropanol and ethanol, it was then tested with non-transparent corpuscular fluids of interest. Specifically, the test was conducted with two different blood samples (AB− and O+ types) using PBS as a buffer. A good signal-to-noise ratio was still achieved even with this more complex fluid at short integration times of 1 second (see ESI† S5). It is possible to distinguish the signal from the two samples using point-like and line excitation configurations, thus paving the way to study diffusion or mixing applications between the two different samples. Having a good signal-to-noise ratio is crucial when developing a high-throughput blood typing protocol using Raman spectroscopy which may benefit from artificial intelligence when assessing the various parameters of the samples.

The continuous development of coherent Raman cytometry platforms will undoubtedly improve the obtainable throughput and enable single-cell analysis of several 100 000 cells within a reasonable timeframe (hours). However, analysis at macro- and bulk scale requires sampling at a much higher rate, *e.g.* monitoring and controlling a range of bioprocesses in biotechnological production.[43] The chip presented in this paper provides a novel method to analyze volumes at this scale.

Conclusions

In this paper, we demonstrated a new method for in-flow whole blood testing, which involves the use of a microfluidic lab-on-a-chip (LoC) based on a hydrodynamic focusing geometry buried in an inert substrate (fused silica). This device, used in conjunction with an optical setup capable of exciting the sample and collecting the Raman signal, showed improved performance and efficiency compared to existing methods. Specifically, the measurement efficiency can be enhanced from analyzing only 8% of the total blood volume with a 100 μm inner diameter capillary, to an efficiency of 100% of the blood flowing inside the chip. This is particularly significant considering diseases linked to the presence of rare cells within the blood composition. Additionally, due to the higher cell speed inside the LoC (for the same flow rate), the intensity threshold at which cell photodegradation begins is raised from 45 kW cm^{-2} (in the case of the capillary) to 245 kW cm^{-2}. These factors enable the use of a 6-times higher excitation power and collection of a 1.5-times higher signal for the same integration time, thereby facilitating faster measurements with our setup. Simultaneously, a higher number of cells is analyzed per unit time, meaning that these measurements are performed on a more statistically significant sample.

The LoC geometry also facilitates Raman multiplexing due to its ease of fabrication. Indeed, multiple hydrofocuses can be created to laminate several liquids in parallel, significantly increasing the device's throughput. It has been demonstrated that signals from different samples are easily distinguishable even in this case. Furthermore, with line laser excitation, by examining the signal intensity at different positions on the spectrometer's CCD camera, it is possible to simultaneously collect signals from different samples without the need for moving parts in the optical setup. The setup has also been tested with non-transparent samples of interest (whole blood from different blood groups), and it was observed that it's possible to acquire Raman spectra with a good signal-to-noise ratio even with relatively short integration times (below 1 second).

The setup described in this work extends beyond merely collecting Raman spectra from different samples. By analyzing

the signal intensity along the *y*-coordinate of the CCD image, it's possible to monitor other significant parameters of the analytes in real-time. For instance, their diffusion within the channel, their mixing, or any reactions occurring between the two samples under examination (or their reactions with the buffer) can be observed.

We believe that the promising results obtained with this setup could pave the way for high-throughput devices for Raman analysis of blood samples in the future. This would allow for easy and rapid access to numerous clinically relevant blood traits, potentially improving the quality of transfusion medicine and enhancing the preventive capacity for diseases related to blood parameters.

Data availability

The data supporting this article have been included as part of the ESI.† Additional data are available upon request.

Author contributions

Conceptualization, A. K., L. C., F. Z., M. S. and S. B.; methodology, A. K. and L. C.; software, E. J.; validation, F. Z., E. J., M. S. and S. B.; formal analysis, F. Z. and E. J.; investigation, F. Z., E. J., M. S.; resources, A. K., L. C., M. H. D.; data curation, F. Z. and E. J.; writing – original draft preparation, F. Z. and E. J.; writing – review and editing, A. K., L. C., M. D., M. S. and S. B.; visualization, F. Z. and E. J.; supervision, A. K. and L. C.; project administration, A. K. All authors have read and agreed to the published version of the manuscript.

Conflicts of interest

The authors declare that they have no personal financial interests or personal relationships that could have caused conflicts of interest in the preparation of this paper.

Acknowledgements

This work was in part supported by a Novo Nordisk Foundation Exploratory Interdisciplinary Synergy Programme Grant, Grant No: NNF21OC0070888.

References

1 T. C. Strekas and T. G. Spiro, *Biochim. Biophys. Acta, Protein Struct.*, 1972, **263**, 830–833.
2 H. Abramczyk and B. Brozek-Pluska, *Anal. Chim. Acta*, 2016, **909**, 91–100.
3 Y. Bai, Z. Yu, S. Yi, Y. Yan, Z. Huang and L. Qiu, *J. Pharm. Biomed. Anal.*, 2020, **190**, 113514.
4 R. Staritzbichler, P. Hunold, I. Estrela-Lopis, P. W. Hildebrand, B. Isermann and T. Kaiser, *PLoS One*, 2021, **16**, e0256045.
5 D. I. Ellis, D. P. Cowcher, L. Ashton, S. O'Hagan and R. Goodacre, *Analyst*, 2013, **138**, 3871.
6 A. Kudelski, *Talanta*, 2008, **76**, 1–8.
7 S. Mosca, C. Conti, N. Stone and P. Matousek, *Nat. Rev. Methods Primers*, 2021, **1**, 21.
8 A. Balzerova, A. Fargasova, Z. Markova, V. Ranc and R. Zboril, *Anal. Chem.*, 2014, **86**, 11107–11114.
9 H. Bian, X. Wang, Y. Yu, X. Wu, D. Chen and J. Gao, *Optik*, 2020, **200**, 163312.
10 E. Mistek, L. Halámková, K. C. Doty, C. K. Muro and I. K. Lednev, *Anal. Chem.*, 2016, **88**, 7453–7456.
11 G. Cheviri, S. Shetty, S. Bharati, S. Chidangil and A. Bankapur, *Anal. Chem.*, 2021, **93**, 5484–5493.
12 L. Rkiouak, M. J. Tang, J. C. J. Camp, J. McGregor, I. M. Watson, R. A. Cox, M. Kalberer, A. D. Ward and F. D. Pope, *Phys. Chem. Chem. Phys.*, 2014, **16**, 11426–11434.
13 D. A. Long, *Raman spectroscopy*, McGraw-Hill, 1977, p. 276.
14 M. J. Pelletier, *Appl. Spectrosc.*, 2003, **57**, 20A–42A.
15 A. Mohan, P. Gupta, A. P. Nair, A. Prabhakar and T. Saiyed, *Biomicrofluidics*, 2020, **14**, 054104.
16 F. Zorzi, S. Bonfadini, L. Aloisio, M. Moschetta, F. Storti, F. Simoni, G. Lanzani and L. Criante, *Sensors*, 2023, **23**, 9191.
17 H. M. Shapiro, *Practical flow cytometry*, John Wiley & Sons, 2005.
18 B. Hansson, C. H. Allen, S. Qutob, B. Behr, B. Nyiri, V. Chauhan and S. Murugkar, *Biomed. Opt. Express*, 2019, **10**, 2275.
19 K. R. Ward, R. W. Barbee, P. S. Reynolds, I. P. T. Filho, M. H. Tiba, L. Torres, R. N. Pittman and J. Terner, *Anal. Chem.*, 2007, **79**, 1514–1518.
20 C. Zhang, T. Uchikoshi, I. Ichinose and L. Liu, *Coatings*, 2019, **9**, 139.
21 Á. Sánchez-Illana, F. Mayr, D. Cuesta-García, J. D. PiñeiroRamos, A. Cantarero, M. de la Guardia, M. Vento, B. Lendl, G. Quintás and J. Kuligowski, *Anal. Chem.*, 2018, **90**, 9093–9100.
22 H. Wang, H. Ma, P. Fang, Y. Xin, C. Li, X. Wan, Z. He, J. Jia and Z. Ling, *Spectrochim. Acta, Part A*, 2021, **259**, 119890.
23 E. A. Jensen, M. Serhatlioglu, C. Uyanik, A. T. Hansen, S. Puthusserypady, M. H. Dziegiel and A. Kristensen, *Adv. Mater. Technol.*, 2024, **9**, 2301462.
24 J. Charles, H. Camp, S. Yegnanarayanan, A. A. Eftekhar and A. Adibi, *Opt. Lett.*, 2011, **36**, 2309.
25 K. Hiramatsu, T. Ideguchi, Y. Yonamine, S. Lee, Y. Luo, K. Hashimoto, T. Ito, M. Hase, J.-W. Park, Y. Kasai, S. Sakuma, T. Hayakawa, F. Arai, Y. Hoshino and K. Goda, *Sci. Adv.*, 2019, **5**, eaau0241.
26 Y. Suzuki, K. Kobayashi, Y. Wakisaka, D. Deng, S. Tanaka, C.-J. Huang, C. Lei, C.-W. Sun, H. Liu, Y. Fujiwaki, S. Lee, A. Isozaki, Y. Kasai, T. Hayakawa, S. Sakuma, F. Arai, K. Koizumi, H. Tezuka, M. Inaba, K. Hiraki, T. Ito, M. Hase, S. Matsusaka, K. Shiba, K. Suga, M. Nishikawa, M. Jona, Y. Yatomi, Y. Yalikun, Y. Tanaka, T. Sugimura, N. Nitta, K. Goda and Y. Ozeki, *Proc. Natl. Acad. Sci. U. S. A.*, 2019, **116**, 15842–15848.
27 N. Nitta, T. Iino, A. Isozaki, M. Yamagishi, Y. Kitahama, S. Sakuma, Y. Suzuki, H. Tezuka, M. Oikawa, F. Arai, T. Asai, D. Deng, H. Fukuzawa, M. Hase, T. Hasunuma, T. Hayakawa, K. Hiraki, K. Hiramatsu, Y. Hoshino, M. Inaba, Y. Inoue, T. Ito, M. Kajikawa, H. Karakawa, Y. Kasai, Y. Kato, H. Kobayashi, C. Lei, S. Matsusaka, H. Mikami, A. Nakagawa, K. Numata, T. Ota, T. Sekiya, K. Shiba, Y. Shirasaki, N. Suzuki, S. Tanaka,

S. Ueno, H. Watarai, T. Yamano, M. Yazawa, Y. Yonamine, D. D. Carlo, Y. Hosokawa, S. Uemura, T. Sugimura, Y. Ozeki and K. Goda, *Nat. Commun.*, 2020, **11**, 3452.
28 F. Storti, S. Bonfadini and L. Criante, *Sci. Rep.*, 2023, **13**, 14671.
29 K. Sugioka and Y. Cheng, *Lab Chip*, 2012, **12**, 3576.
30 R. Martínez-Vásquez, F. Bragheri and P. Paié, *New Trends and Applications in Femtosecond Laser Micromachining*, MDPI, 2022.
31 R. R. Gattass and E. Mazur, *Nat. Photonics*, 2008, **2**, 219–225.
32 J. Qiu, K. Miura and K. Hirao, *J. Non-Cryst. Solids*, 2008, **354**, 1100–1111.
33 A. Marcinkevičius, S. Juodkazis, M. Watanabe, M. Miwa, S. Matsuo, H. Misawa and J. Nishii, *Opt. Lett.*, 2001, **26**, 277.
34 C. Hnatovsky, R. S. Taylor, E. Simova, V. R. Bhardwaj, D. M. Rayner and P. B. Corkum, *Opt. Lett.*, 2005, **30**, 1867.
35 J. Gottmann, *J. Laser Micro/Nanoeng.*, 2013, **8**, 15–18.
36 M. Hermans, *J. Laser Micro/Nanoeng.*, 2014, **9**, 126–131.
37 D. A. Yashunin, Y. A. Malkov, L. A. Mochalov and A. N. Stepanov, *J. Appl. Phys.*, 2015, **118**, 093106.
38 A. Campion, *Vibrational Spectroscopy of Molecules on Surfaces*, Springer US, 1987, pp. 345–415.
39 G. Keresztury, *Raman Spectroscopy: Theory*, 2001.
40 D. Lin, L. Shen, M. Luo, K. Zhang, J. Li, Q. Yang, F. Zhu, D. Zhou, S. Zheng, Y. Chen and J. Zhou, *Signal Transduction Targeted Ther.*, 2021, **6**, 404.
41 D. Hanahan and R. A. Weinberg, *Cell*, 2011, **144**, 646–674.
42 S. Ahlawat, N. Kumar, A. Uppal and P. K. Gupta, *J. Biophotonics*, 2017, **10**, 415–422.
43 K. A. Esmonde-White, M. Cuellar and I. R. Lewis, *Anal. Bioanal. Chem.*, 2022, **414**, 969–991.